REPORT DOCUMENTATION PAGE

Form Approved OMB NO. 0704-0188

1. REPORT DATE (DD-MM-YYYY)	2. REPORT TYPE	3. DATES COVERED (From - To)
	New Reprint	-

4. TITLE AND SUBTITLE	5a. CONTRACT NUMBER
Tuning Energetic Material Reactivity Using Surface Functionalization of Aluminum Fuels	W911NF-11-1-0439
	5b. GRANT NUMBER
	5c. PROGRAM ELEMENT NUMBER
	611102

6. AUTHORS	5d. PROJECT NUMBER
Keerti S. Kappagantula, Cory Farley, Michelle L. Pantoya, Jillian Horn	
	5e. TASK NUMBER
	5f. WORK UNIT NUMBER

7. PERFORMING ORGANIZATION NAMES AND ADDRESSES	8. PERFORMING ORGANIZATION REPORT NUMBER
Texas Technical University Box 41035 349 Admin Bldg Lubbock, TX 79409 -1035	

9. SPONSORING/MONITORING AGENCY NAME(S) AND ADDRESS(ES)	10. SPONSOR/MONITOR'S ACRONYM(S)
U.S. Army Research Office P.O. Box 12211 Research Triangle Park, NC 27709-2211	ARO
	11. SPONSOR/MONITOR'S REPORT NUMBER(S)
	58857-EG.25

12. DISTRIBUTION AVAILIBILITY STATEMENT

Approved for public release; distribution is unlimited.

13. SUPPLEMENTARY NOTES

The views, opinions and/or findings contained in this report are those of the author(s) and should not contrued as an official Department of the Army position, policy or decision, unless so designated by other documentation.

14. ABSTRACT

Combustion analysis of three different thermites consisting of aluminum (Al) particles with and without surface functionalization combined with molybdenum trioxide (MoO3) was performed to study the effect of surface functionalization on flame propagation velocity (FPV). Two types of Al particles had self-assembled monolayers (SAMs) of perfluoro tetradecanoic (PFTD) and perfluoro sebacic (PFS) acids around the alumina shell, respectively; the other one did not. Flame speeds for Al with PFTD acid combined with MoO3 are 86% higher than

15. SUBJECT TERMS

aluminum surface functionalization, tunability of thermites, aluminum synthesis, aluminum fluoropolymer combustion, acid coatings

16. SECURITY CLASSIFICATION OF:			17. LIMITATION OF ABSTRACT	15. NUMBER OF PAGES	19a. NAME OF RESPONSIBLE PERSON
a. REPORT	b. ABSTRACT	c. THIS PAGE	UU		Michelle Pantoya
UU	UU	UU			19b. TELEPHONE NUMBER
					806-742-3563

Standard Form 298 (Rev 8/98)
Prescribed by ANSI Std. Z39.18

Report Title

Tuning Energetic Material Reactivity Using Surface Functionalization of Aluminum Fuels

ABSTRACT

Combustion analysis of three different thermites consisting of aluminum (Al) particles with and without surface functionalization combined with molybdenum trioxide (MoO3) was performed to study the effect of surface functionalization on flame propagation velocity (FPV). Two types of Al particles had self-assembled monolayers (SAMs) of perfluoro tetradecanoic (PFTD) and perfluoro sebacic (PFS) acids around the alumina shell, respectively; the other one did not. Flame speeds for Al with PFTD acid combined with MoO3 are 86% higher than Al/MoO3 whereas those for Al with PFS acid combined with MoO3 are almost half of Al/MoO3. The Al?PFTD structure is more sterically hindered and exhibits lower bond dissociation energy. This chemistry promotes increased flame speeds. Thermal equilibrium studies were performed
using a differential scanning calorimeter and a thermogravimetric analyzer to determine activation energy (Ea) of the thermites. Results are consistent with flame speed observations and showed an inverse relationship between flame speed and Ea. This study shows that surface functionalization can be used as an approach to control the reactivity of Al particles.

REPORT DOCUMENTATION PAGE (SF298)
(Continuation Sheet)

Continuation for Block 13

ARO Report Number   58857.25-EG
Tuning Energetic Material Reactivity Using Surfa   ...
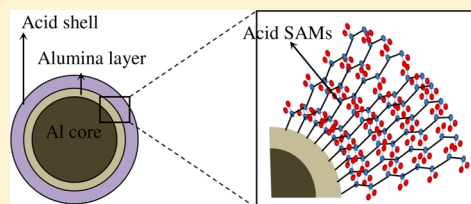
Block 13: Supplementary Note

Tuning Energetic Material Reactivity Using Surface Functionalization of Aluminum Fuels

Keerti S. Kappagantula,[†] Cory Farley,[†] Michelle L. Pantoya,[*,†] and Jillian Horn[‡]

[†]Department of Mechanical Engineering, Texas Tech University, Lubbock, Texas 79409, United States
[‡]Naval Surface Warfare Center—Indian Head Division, Research and Technology Department, Indian Head, Maryland 20640, United States

ABSTRACT: Combustion analysis of three different thermites consisting of aluminum (Al) particles with and without surface functionalization combined with molybdenum trioxide (MoO_3) was performed to study the effect of surface functionalization on flame propagation velocity (FPV). Two types of Al particles had self-assembled monolayers (SAMs) of perfluoro tetradecanoic (PFTD) and perfluoro sebacic (PFS) acids around the alumina shell, respectively; the other one did not. Flame speeds for Al with PFTD acid combined with MoO_3 are 86% higher than Al/MoO_3 whereas those for Al with PFS acid combined with MoO_3 are almost half of Al/MoO_3. The Al—PFTD structure is more sterically hindered and exhibits lower bond dissociation energy. This chemistry promotes increased flame speeds. Thermal equilibrium studies were performed using a differential scanning calorimeter and a thermogravimetric analyzer to determine activation energy (E_a) of the thermites. Results are consistent with flame speed observations and showed an inverse relationship between flame speed and E_a. This study shows that surface functionalization can be used as an approach to control the reactivity of Al particles.

INTRODUCTION

Composite energetic materials consisting of solid metal fuel and oxidizer particles are referred to here as thermites. In general, aluminum (Al) is a preferred fuel owing to its high oxidation energy, and micrometer Al is often a reactant in composite energetic materials. The oxidation process for thermites is diffusion limited such that the mass transport and diffusion distances control the energy release rate. The increase in specific surface area and number of contact points between fuel and oxidizer that is gained by replacing micrometer Al with nanometer Al has a profound effect on the thermite's reactivity and has been studied extensively.[1,2] Thermites with nanoscale particles are sometimes referred to as metastable interstitial composites (MIC), or simply, nanocomposites. Nanometric reactants have reaction velocities that are orders of magnitude greater than their micrometer counterparts.[3] In addition to these advantages, nanocomposites also have lower ignition delays and high ignition sensitivity.[4]

Although a decrease in the reactant size enhances reactivity, there are several problems associated with nanometric reactants. The higher surface energy of the nanoparticles leads to greater particle aggregation (in order to minimize the free energy of the system), which makes homogenizing the composite difficult.[5] Another issue associated with the high surface area of the nanoparticles is the increased amount of viscosity when the nanoparticles are introduced into a solvent during composite preparation, which can lead to unwanted friction generation during particle mixing and increased composite agglomeration.[6] Apart from these, however, one of the biggest problems is excessive oxidation of the fuel particle (Al) before combustion.[7] In general, nano Al particles have a

passivating alumina (Al_2O_3) shell with an average thickness of 1.7 to 6.0 nm,[8] which accounts for almost 25—40% of the entire volume, depending on the particle size. Although the oxide layer is an inert coating, prolonged exposure to air or moisture will further oxidize the Al particle, thus depleting the active Al content over time, thereby aging the fuel.

One technique to counter these problems is chemical functionalization of the nanoparticle surface. In general, surface functionalization refers to the process of encompassing the nanoparticles in an organic corona. Because the Al particles have a surrounding Al_2O_3 shell, the material used for surface functionalization should be capable of interacting either physically or chemically with the alumina shell. Under standard atmospheric conditions, the Al_2O_3 shell can become partially hydroxylated,[9] providing an additional route for surface functionalization. Ample literature is available about the chemical functionalization of Al_2O_3 oxide on bulk Al particles using the condensation of carboxylic acids to surface bound hydroxyls in order to form self-assembled monolayers (SAMs).[10−12] Successful functionalization of alumina with silanes,[13] phosphoric acids,[14] and hydroxamix acids[15] has been demonstrated. Research shows that the physical properties of these nanoparticles are functions of the physical and chemical compositions of the surface corona to a great extent.[16,17]

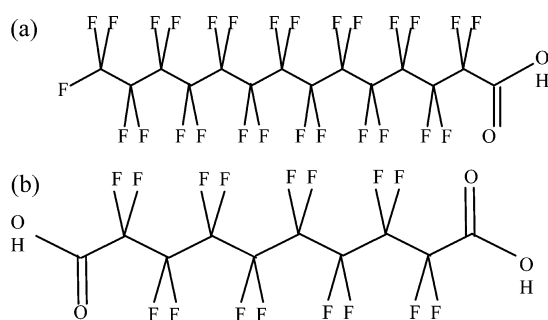Developing new Al-based nanocomposite systems that possess energetic properties tailored for a desired application

often requires the use of very large particle loadings. This has been achieved by using perfluoroalkyl carboxylic acids,[6] silanes,[18] and glycols[19] among others. It was seen that the combustion performance of such Al nanocomposites was affected by the presence of functional groups on these particles; combustion velocities of such nanocomposites decreased with the presence of hydroxyl groups.[20]

Surface functionalization of Al nanoparticles without the alumina shell was achieved too.[6] However, flame propagation studies of thermites made with such Al particles showed that their flame propagation velocity (FPV) was low compared to thermites consisting of Al with an alumina shell and no surface functionalization.[20] In addition, the method of preparation of such perfluoroalkyl carboxylic acid coated Al particles without the alumina shell was deemed unfit for mass production because partial fluorine passivation led to an extremely pyrophoric material.

Perfluoroalkyl acids are particularly interesting as coatings over Al particles because using fluorinated compounds offers an added increase in energy content of the system during combustion because fluorine can act as an oxidizer for aluminum. In fact, the formation of AlF_3 releases 55.67 kJ/g, which is a significant increase over the formation of Al_2O_3 (30.96 kJ/g).[21] In an effort to capitalize on this potential, nano Al particles with an Al_2O_3 shell were coated with fluoropolymer acids, and their resulting reaction kinetics were examined.[22] Experiments were performed to assess reactivity in terms of activation energy (E_a) and flame propagation velocity (FPV) of loose powder mixtures consisting of an Al sample combined with molybdenum trioxide (MoO_3).

■ MATERIALS

Three different types of Al each with 80 nm average particle diameter were used as fuels. All the Al particles were encapsulated in an alumina (Al_2O_3) passivation shell with an average thickness of 2.7 nm. Aluminum particles referred to as Al−PFTD hence forth had a 5 nm thick layer of perfluorotetradecanoic acid (PFTD) over the Al_2O_3 shell. Similarly, particles referred to as Al−PFS hence forth had a 5 nm thick layer of perfluoro sebacic acid (PFS) over the Al_2O_3 shell. It is noted that these acids do not bond to the alumina shell but cut channels in the alumina to bond with the Al core. In this way, the coating surrounds the alumina as hairlike chains. The third sample of Al particles had an alumina passivation shell without acid coating and will be referred to as Al. The structures of PFTD and PFS acids are shown in Figure 1. Table 1 shows the alumina shell thickness, acid layer thickness, and acid concentration of the fuel particles.

Figure 1. Schematic representation of the chemical structure of the PFTD and PFS acids, respectively.

Table 1. Physical and Chemical Specifications of the Al Fuel Particles

material	particle size (nm)	oxide layer thickness (nm)	acid layer thickness (nm)	acid content (% wt)
Al	80	2.7	n/a	n/a
Al−PFTD	80	2.7	5	35%
Al−PFS	80	2.7	5	35%

The Al nanoparticles used throughout this study were procured from Nova Centrix Corp. (Austin, TX, USA). These Al particles were coated with PFTD acid to obtain Al−PFTD and with PFS acid to obtain Al−PFS, respectively, in a slurry of diethyl ether. The powder product was washed three times in diethyl ether to remove any acid that was not bonded to the alumina shell. The end result was Al particles with a perfluoroalkyl acid SAM surrounding the Al_2O_3 shell. The detailed preparation method for these acid-coated Al particles may be obtained elsewhere.[22] It was proposed that the perfluoroalkyl acids, PFTD and PFS, bond to the alumina through the carboxylic functional group.[6]

Molybdenum trioxide (MoO_3) procured from Mach I (USA) was used as the oxidizer. The MoO_3 particles have an average thickness of 44 nm with rectangular platelike morphology, whereas the Al particles are spherical.

■ EXPERIMENTAL SECTION

The redox reactions between Al, the acid shell, and MoO_3 are complex and not well understood. Hence, the reactant concentrations are expressed in terms of mass percentages and not in terms of equivalence ratio. Previous work by Dikici et al. showed that Al/MoO_3 has the highest FPV at a 70.6% by mass MoO_3, and the same Al/MoO_3 ratio was adopted here.[20]

For preparing the thermites, requisite amounts of Al fuel (with and without acid coatings) and MoO_3 oxidizer were measured and suspended in hexanes. The suspension was then sonicated using a Misonix Sonic wand for 120 s in 10 s intervals. Sonication helps break agglomerates and improves homogeneity of the composite. The hexanes suspension was transferred to a Pyrex dish and heated to a temperature of 45 °C to facilitate the evaporation of hexane. Once the powder mixture dried, it was reclaimed for further experimentation. Thus, three thermites were prepared corresponding to the three different Al fuels.

Flame Propagation Experiments. Flame propagation experiments were conducted using the three thermites to determine the FPV. The flame tube apparatus used, popularly known as the "Bockmon tube", was first designed by Bockmon et al.[23] and is used extensively in flame propagation experiments.[20,24−26] A modified version of this was used in the current work. It consisted of a quartz tube, 110 mm long, with an inner diameter of 3 mm and an outer diameter of 8 mm. The dimension of the inner diameter of the tube was chosen to be small enough in comparison to the length of the tube to ensure sufficient heat transfer only along the length of the tube; heat transfer along the radius may be considered negligible. The transparency of quartz allows visual inspection of the flame front during reaction.

Each thermite was loaded into the tube and placed on a vibrating block for 5 s to reduce local density gradients. Each tube contained about 468 ± 10 mg of thermite resulting in a loose powder fill estimated to be 7% of the theoretical

maximum density. Once prepared, the tube was placed in a steel combustion chamber, and the experimental setup is schematically represented in Figure 2.
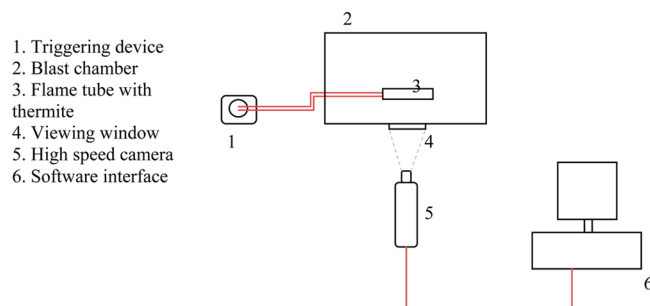

1. Triggering device
2. Blast chamber
3. Flame tube with thermite
4. Viewing window
5. High speed camera
6. Software interface

Figure 2. Experimental setup for measuring FPV.

Thermite ignition was via thermal stimulus provided by a Nichrome wire connected to an external voltage supply. A Phantom v7 (Vision Research, Inc., Wayne, NJ, USA) with a Nikon AF Nikkor 52 mm 1:2.8 lens was used to record ignition and flame propagation. The camera captured images of the reacting composite, perpendicular to the direction of flame propagation, at a speed of 160 000 frames per second, with a resolution of 256 by 128 pixels. Vision Research software was used to postprocess the recorded photographic data. When a reference length is established, the software determines speed based on a distance between sequential time frames. Using a "find-edge" image filter that identifies preset variations in pixel intensity, the flame front location (which is identified as the region of the flame with the maximum radiance) is identified and marked for speed measurements.

Thermal Equilibrium Experiments. Activation energy was found using a thermoequilibrium isoconversion method. Samples of approximately 6 mg were loaded into a Neztsch STA 409 differential scanning calorimeter (DSC) and thermogravimetric analyzer (TGA) and heated to 1273 K at 2, 5, or 10 K/min in a 1:3 (by volume) oxygen−argon environment. Within the DSC/TGA, the sample crucible is compared to an empty reference crucible in order to obtain the net energy and mass change. Also, the sample carrier was mounted on a microscale (i.e., TGA) allowing for mass change measurements that relay phase change (i.e., gas production) information as a function of equilibrium temperature. The slope of the DSC curve changes when the reaction within the DSC/TGA produces enough energy to become noticeable within the natural noise of the machine. The area under the DSC curve corresponds with the net exothermic behavior. The activation energies were then calculated using eq 1 from the Type B-1.95 peak method as described by M.J. Starink.[27]

$$\frac{B}{T_p^{1.95}} = A \exp\left(-\frac{E_a}{RT_p}\right)$$

(1)

In eq 1, B is the heating rate, A is the pre-exponential factor, E_a is the activation energy, R is the universal gas constant, and T_p is the temperature at the exothermic peak of the reaction. Reaction rate is approximated by $B/T_p^{1.95}$. Taking the natural log yields eq 2.

$$\ln\left(\frac{B}{T_p^{1.95}}\right) = -\frac{E_a}{RT_p} + \ln A$$

(2)

By plotting $\ln(B/T_p^{1.95})$ as a function of $(1/RT_p)$ for the different heating rates, E_a (kJ/mol) can be found as the slope of the trend line.

The isoconversion approach requires the identification of an inflection point in the heat flow curves that is consistently present for all heating rates. In this study, this isoconversion point corresponds to an initial and perhaps rate-determining step in the reaction such that differences in the subsequent reaction mechanism associated with equilibrium versus non-equilibrium experiments do not influence the activation energy analyses.

■ RESULTS

Three tubes were prepared for each thermite allowing for an estimate of the repeatability and uncertainty in the measurement. The FPV was measured at distances sufficiently away from the Nichrome wire location such that the flame attained a steady-state velocity. The activation energy for these samples as well as their FPV are shown in Table 2. The FPV of Al−PFTD/MoO$_3$ is 86% faster than that of Al/MoO$_3$, whereas the FPV of Al−PFS/MoO$_3$ is almost half that of Al/MoO$_3$.
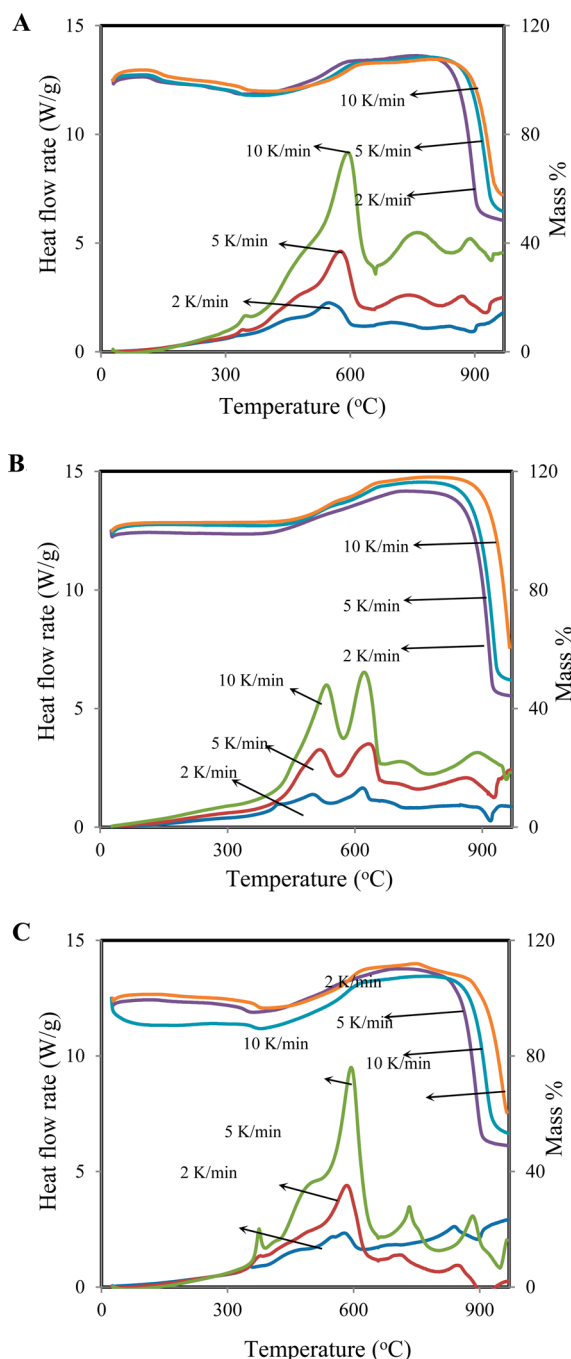
Table 2. Flame Propagation Velocity (FPV) and Activation Energy (E_a) of Thermite Samples

test no.	material	E_a (kJ/mol)	mass of the powder in the flame tube	FPV (m/s)	av FPV (m/s)
1	Al/MoO$_3$	252	464.7	262.1	267.3 ± 5.2
2			469.9	269.3	
3			457.3	270.4	
4	Al−PFTD/MoO$_3$	185	463.4	496.3	497.3 ± 4.6
5			460.2	501.9	
6			456.5	493.7	
7	Al−PFS/MoO$_3$	553	483.9	138.9	137.8 ± 1.8
8			474.1	136.0	
9			476.6	137.5	

Figure 3A−C shows the DSC/TGA plots of the three thermites as a function of temperature at three different heating rates: 2, 5, and 10 K/min. The Al−PFTD/MoO$_3$ and Al−PFS/MoO$_3$ reactions show a smaller exotherm before the bigger one whereas the same is not seen in the Al/MoO$_3$ reaction plot. Also, two small endotherms are to be noted on the DSC plots of the thermites with acid-coated fuels at about 650−660 °C. This temperature corresponds to the melting point of Al, which might mean that the endotherm may represent the melting of some excess Al left over after it reacts with the MoO$_3$ present. Such an endotherm is not present in the Al/MoO$_3$ DSC plots; however, there is a second endotherm present in the Al/MoO$_3$ plot signifying two reactions occurring at two different temperatures. It may be concluded that the first peak corresponds to the oxidation of Al with MoO$_3$ particles, which is known to occur at around 540 °C.[28] In order to understand the second peak of the heat curve, a DSC scan of the same thermite was performed with the identical sample size and heating rate in an exclusively argon (Ar) environment. The resultant heat curve is shown in Figure 4.
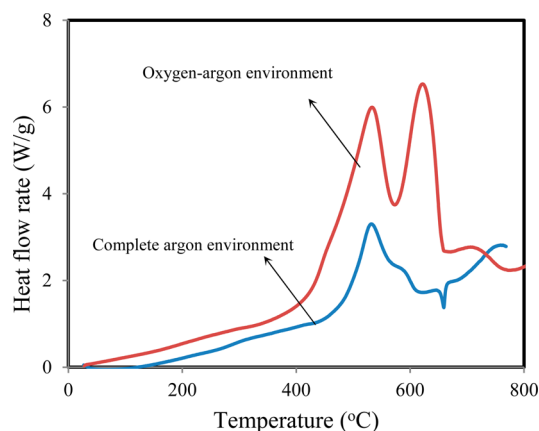
The Al/MoO$_3$ combustion in an Ar environment shows an endothermic dip at about 660 °C, (corresponding to unburned Al melting). By comparing this to the heat curve initially observed for Al/MoO$_3$ (Figure 4) combustion in an oxygen−argon environment, it may be seen that the second exothermic
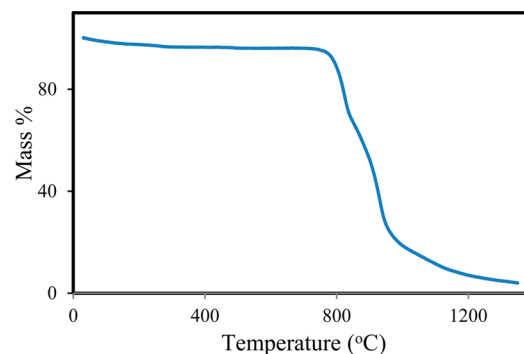
Figure 3. (A) DSC (three plots on the bottom)/TGA (three plots on the top) of the Al–PFTD/MoO₃ reaction at different heating rates. (B) DSC (three plots on the bottom)/TGA (three plots on the top) of the Al/MoO₃ reaction at different heating rates. (C) DSC (three plots on the bottom)/TGA (three plots on the top) of the Al–PFS/MoO₃ reaction at different heating rates.

Figure 4. Heat flow curve of Al/MoO₃ thermite as a function of temperature for a constant 10 K/min heating rate.

be oxidized in the oxygen environment upon further heating. This oxidation of Al by oxygen will result in an exotherm. Therefore, the second exothermic peak in the heat curve of Al/MoO₃ is due to the unburned Al particles oxidized by oxygen in the environment. Another interesting observation from Figure 3A–C is a mass loss of 40–50% for every thermite sample starting at around 800 °C. Figure 5 is a TGA scan of MoO₃
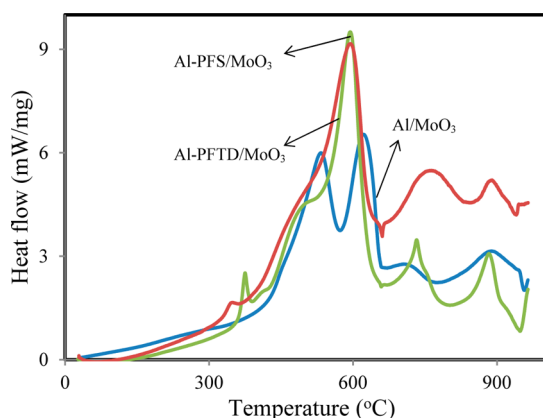

Figure 5. TGA curve of MoO₃ as a function of temperature for a constant 10 K/min heating rate and in an oxygen–argon environment.

performed in a 1:3 (by volume) oxygen–argon environment that shows a mass loss starting at about 790 °C corresponding to sublimation of MoO₃. The mass loss in Figure 5 is similar to the mass loss observed in Figure 3A–C and also can be attributed to the sublimation of MoO₃, which occurs at 795 °C.
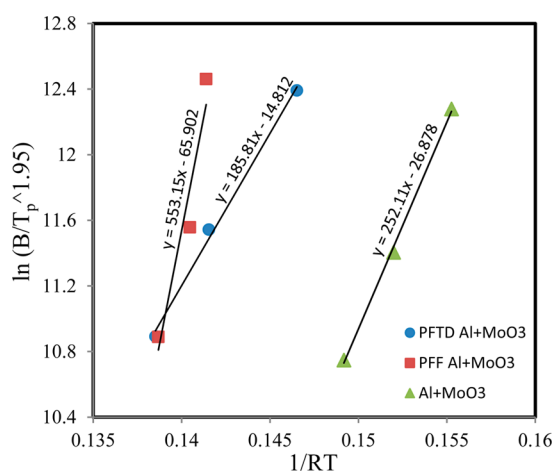
For ease of comparison, the DSC plots of all the thermites for a constant 10 K/min heating rate are provided together in Figure 6.

In Figure 6, the first exotherm for Al–PFTD/MoO₃ occurs at a lower temperature than the first exotherm for Al–PFS/MoO₃. The analysis in Figure 6 is extended to lower heating rates in order to measure the isoconversion temperature corresponding to a continuous transition. By using the values for peak temperature (T_p) at various heating rates (i.e., 2, 5, and 10 K/min), the $\ln(B/T_p^{1.95})$ as a function of $(1/RT_p)$ for each thermite was plotted, and the results are shown in Figure 7.

The slopes of the trend lines in Figure 7 are the activation energies (E_a) for each thermite. It is noted that Table 2 shows the E_a of Al/MoO₃ is 252 kJ/mol, corresponding to the E_a values found in literature.[29,30] The interesting point to note is that the activation energy trend is opposite to that of the FPV

peak corresponds with the Al melt endotherm. In an entirely argon environment, the only oxidizer available during the reaction would be MoO₃. Once all the MoO₃ is consumed in reaction with Al, unreacted Al particles cannot react with any other oxidizer and hence melt when heated further. On the other hand, in a 1:3 (by volume) oxygen–argon environment, the Al particles have two oxidizers to react with: MoO₃ mixed in the thermite *and* oxygen in the environment. Therefore, Al left behind after MoO₃ is consumed in the redox reaction may

Figure 6. DSC curve of each thermite as a function of temperature for a constant 10 K/min heating rate.

Figure 7. Trend lines showing the activation energy of the thermite compositions.

values, that is, thermites with low FPV have high E_a and vice versa. Since parameters such as flame tube diameter, length, Al and MoO_3 mass percentages, TMD, and stimulus voltage were maintained constant, the contributing factor for the difference in the FPV may be the chemical composition and kinetics of the acid shell.

DISCUSSION

Osborne and Pantoya[31] showed that, when Al reacts with polytetrafluoroethylene (Teflon), the fluorine radicals formed at elevated temperatures react with the Al_2O_3 shell in the presence of hydroxyl groups leading to the formation of aluminum fluoride (AlF_3). This interaction occurs during a preignition reaction (PIR) at about 400 °C, identified as a small exotherm on the DSC plot at that temperature. They postulated that the formation of AlF_3 serves to degrade Al_2O_3 leaving the particle core exposed for further reaction. The acid coatings used here contain a large percentage of fluorine in their alkyl chains terminating in carboxylic groups as illustrated in Figure 1; PFTD acid contains 72% fluorine by weight whereas PFS acid has 62% fluorine be weight. At elevated temperatures, the fluorine radicals in gaseous form may react with Al_2O_3 (similar to fluorine radicals from Teflon molecules) degrading the alumina shell and exposing the Al core for further oxidation. The small exotherms on the DSC plots in Figures 3A, C and 6 are identified as PIRs (similar to the exotherms on

the DSC plot of Al/Teflon reaction).[31] The Al−PFTD/MoO_3 exhibits a PIR onset at 320 °C and a peak at 342 °C while the Al−PFS/MoO_3 exhibits a PIR onset at 350 °C and a peak at 374 °C. After the PIR in Figure 6, the heat flow curves appear similar, and there is no further indication of discrepancies in the equilibrium kinetics that account for the differences in FPV seen in Table 2 (i.e., 86% increase over Al/MoO_3 in the case of Al−PFTD/MoO_3 and 48% decrease in the case of Al−PFS/MoO_3).

It should be noted that, although there is a mass loss during the thermoequilibrium tests in the DSC due to the sublimation of MoO_3 at ∼790 °C, a similar phenomenon may not occur during the flame tube experiments. In the DSC, nearly equilibrium conditions exist, and often reactions are not complete. At heating rates on the order of 10 K/min, there is plenty of time for any gaseous species to escape from the chamber prior to reacting. Similarly, in this study, enough MoO_3 is available prior to its sublimation to react with Al and produce the observed exotherms. The DSC data provides some insight into the possible reaction mechanism that may still be applicable to the higher heating rate conditions associated with the flame propagation in the tube. This is particularly useful for the two acid-coated Al samples, which indicate distinctly different onset temperatures for a PIR that may correlate to dramatically different FPVs. It is also noted that, in the flame tube experiments, the heating rates are many orders of magnitude higher than DSC and, since the reaction progresses in a confined environment, the sublimed MoO_3 is likely more readily available and not escaping as in the DSC.

An interesting interpretation from Figure 3A−C, Figure 6, and Table 2 is that the acid coating may be tailored to sensitize or desensitize the thermite. In the case of PFTD, the coating appears to enhance ignition sensitivity by (1) reducing the onset of the PIR, (2) producing lower activation energy, and (3) promoting higher flame speeds. PFTD acid has a longer −CF_2− chain compared to PFS acid (Figure 1). Longer chains are less stable and faster to react because they more readily form radicals compared to acids with smaller chains.[32] Also, PFTD acid contains higher percent by weight of fluorine (72% compared to 62% in PFS acid), which is a highly electronegative oxidizer. Pantoya and Dean[33] showed that the Al−F PIR is directly correlated with fluorine concentration and the specific surface area of the Al particle. Higher fluorine concentrations and specific surface areas lead to a lower PIR onset. This is also seen in Figure 6 with a 30 °C reduction in onset PIR with PFTD compared with PFS. Reducing the onset for the PIR may promote Al oxidation and contribute toward understanding the observation of increased FPV of Al−PFTD/MoO_3 compared to that of Al−PFS/MoO_3. Controlling the PIR onset may be critical to controlling the reactivity of the acid-coated Al thermite.

Furthermore, the PFS acid is a more symmetrically stable molecule compared to the PFTD acid. Therefore, bond breaking and radical formation from PFS requires more energy than PFTD resulting in higher E_a. Also, oxygen and hydrogen from the PFS carboxylic group may bond with fluorine radicals at the reaction front, further decreasing the concentration of fluorine available, consequently inhibiting Al oxidation and decreasing the FPV of the Al−PFS/MoO_3. The PFS molecule is less sterically hindered at its end, having an extra carboxylic acid functional group, consisting of a π bond between carbon and oxygen. Although the —C—F— is one of the strongest single bonds with a bond dissociation energy (BDE) of 490 kJ/

mol, the —C≡O— is a π bond with a higher BDE of about 799−802 kJ/mol.[32] This means that almost twice the amount of energy required to cleave a —C—F— bond is necessary to cleave a —C≡O— bond, which may also account for the higher E_a of Al−PFS/MoO₃ and the delayed PIR observed in Figure 3C. Thadhani et al.[34] showed that, for solid-state reactants, a reduced onset temperature would imply a higher reaction rate. It is very interesting to note that results from this study are consistent with Thadhani et al. such that the onset temperature for Al−PFTD/MoO₃ is lower than Al−PFS/MoO₃ and the corresponding FPV is similarly correlated.

An interesting finding from this study is that the additional gas generated by the acid coatings can have a dual affect. In one case, the fluorine containing gas may accelerate the reaction through surface chemistry likely associated with fluorine attacking the alumina passivation shell. This coupled with a higher level of gas generation may further promote the flame front propagation through enhanced convection. In the other case, the molecular chemistry of the acid chain acts to retard the flame speed possibly because of the bidentate nature of the surface bond and/or because the chain is inherently stronger. Even though this produced a flame speed only about half as much as the uncoated Al mixture, the gas generated from the coating still contributes toward a convectively driven reaction. In both cases, the gas generation behaviors of the acid-coated fuels contribute to the overall reactivity of the mixture.

The FPV and E_a have an inverse relationship for the three thermites (Table 2). Activation energy measured here is apparent activation energy because the measurement considers influences beyond stoichiometry. The apparent activation energy quantifies the energy barrier needed to be overcome in order for a chemical reaction to occur. Reactants having high activation energy require greater energy input compared to reactants with lower activation energy.

Combustion of a thermite in a flame tube proceeds along the lateral axis of the flame tube. Given that the diameter of the flame tube is smaller than its length by an order of magnitude, heat transfer during the reaction may be approximated as one-dimensional. Thermal stimulus via Nichrome wire heats up the portion of thermite in its vicinity, increasing the energy of the reactants above their activation energy. An exothermic reaction starts during the oxidation of the fuel. Energy released during this oxidation reaction heats the thermite adjacent to the reaction zone. Once the adjacent reactants obtain energy greater than its activation energy, the fuel and oxidizer particles start reacting exothermally. Thus, the reaction propagates in a flame tube. This progression of the reaction manifests itself as a fast moving flame front that can be observed visually. Thermites with low activation energy require comparatively less energy to overcome the E_a barrier. This implies that energy is more readily transferred to (rather than consumed by) unreacted thermite, and the result is faster propagation of the reaction and higher FPV. On the other hand, thermites with comparatively higher E_a consume more energy at the reaction site and result in lower FPV. This is exactly mirrored in the results as can be seen from Table 2.

It is interesting to note that the FPV values recorded for Al/MoO₃ are different from those observed previously.[20,23] This may be due to the differences in equivalence ratio. In the current work, 70.6% MoO₃ by weight was maintained in the thermite samples consistently, which corresponds to an equivalence ratio of 0.9. A different equivalence ratio greatly influences the FPV, and since the difference is on the fuel lean side, the slower flame speed is consistent with what is expected. It should be noted that the MoO₃ used in the current work is the same as the one used by Dikici et al.[20] This implies that the oxidizer aged by almost four years. The effects of aging and exposure to humidity on oxidizers are not well understood, but this may be another contributing factor to the difference in velocities. In this study, however, the parameters held constant are the fuel and oxidizer weight percentages and the oxidizer used to prepare the thermites such that significance is placed on the dramatically different combustion behaviors associated with the acid coatings and, regardless of numerical values of overall FPV or E_a, the trends are expected to remain constant and be valid for extended research and application.

■ CONCLUSIONS

Thermal equilibrium and flame propagation experiments were performed for three thermites each containing 80 nm average diameter Al particles combined with MoO₃. Two thermites contained Al-coated particles with different acids and an uncoated Al thermite was used as a baseline for comparison. The acids were SAMs of PFTD and PFS such that the thermites were labeled Al−PFTD/MoO₃, Al−PFS/MoO₃, and Al/MoO₃. Results showed that Al−PFTD/MoO₃ had the highest velocity and almost double that of Al/MoO₃. On the other hand, Al−PFS/MoO₃ had the lowest velocity and only 48% as high as that of Al/MoO₃. Equilibrium analyses revealed that the PFTD acid promoted a lower onset for a PIR, which may be spurred by reduced structural stability of the acid molecular chain (i.e., more sterically hindered). The lower onset for the fluorine aluminum PIR was a significant difference in the heat flow trends for the two different acid coatings and may be an indication of a key parameter controlling reactivity of the acid coated Al.

Activation energy showed an inverse trend with velocity, with highest velocity associated with the lowest E_a. This finding was anticipated because propagation velocity can be described as a series of ignition sites such that lower activation energy correlates with higher propagation velocity for the similar thermites examined here.

These findings are impactful because they suggest that the structure of the acid coating can be tailored to enhance or reduce the reactivity of the thermite. Results suggest that, because the PFTD coating is less stable and contains a higher concentration of fluorine, these factors promote an earlier onset of a PIR that enhances thermite reactivity (in terms of higher velocity and lower activation energy). On the other hand, PFS is more stable, requires greater bond energy for dissociation, and results in a delayed onset for the PIR, higher activation energy, and lower flame speeds, reducing the overall thermite reactivity.

■ AUTHOR INFORMATION

Corresponding Author
*Phone: (806) 742-3563; e-mail: michelle.pantoya@ttu.edu.

Author Contributions
The manuscript was written through contributions of all authors. All authors have given approval to the final version of the manuscript.

Notes
The authors declare no competing financial interest.

■ REFERENCES

(1) Wang, L.; Munzir, Z.; Maximov, Y. *J. Mater. Sci.* **1993**, *28*, 3693−3708.

(2) Shimizu, A.; J. Saitou, J. *Solid State Ionics* **1990**, *38*, 261−269.

(3) Granier, J.; Pantoya, M. L. *Propellants, Explos., Pyrotech.* **2005**, *30*, 53−62.

(4) Engelen, K.; Vanneste, L.; Lefebvre, M. H. *Twenty-Eighth International Pyrotechnics Seminar, Adelaide, South Australia, 4−9 November 2001*; Weapons Systems Division, Defence Science and Technology Organisation: Australia, 2001.

(5) Brege, J.; Hamilton, C.; Crouse, C.; Barron, A. *Nano Lett.* **2009**, *9* (6), 2239−2242.

(6) Jouet, R. J.; Warren, A.; Rosenberg, D. M.; Bellito, V. J.; Park, K.; Zachariah, M. *Chem. Mater.* **2005**, *17*, 2987−2996.

(7) Brewer, R.; Dixon, P.; Ford, S.; Higa, K.; Jones, R. *Lead Free Electric Primer*, Final Technical Report; Naval Air Warfare Center, Weapons Division: China Lake, CA, 2006.

(8) Pesiri, D.; Aumann, C.; Bilger, L.; Booth, D.; Carpenter, R.; Dye, R.; O'Neill, E.; Shelton, D.; Walter, K. *J. Pyrotech.* **2004**, *19*, 19−32.

(9) Wefers, K.; Misa, C. *Tech. Pap. − Alcoa Res. Lab.* **1988**, *19*.

(10) Oberg, K.; Persson, P.; Shchukarev, A.; Eliasson, B. *Thin Solid Films* **2001**, *397*, 102−108.

(11) Lee, M.; Feng, K.; Chen, X.; Wu, N.; Raman, A.; Nightingale, J.; Gawalt, E.; Korakakis, D.; Hornak, L.; Tiperman, A. *Langmuir* **2007**, *23* (5), 2444−2452.

(12) Karaman, M. E.; Antelmi, D. A.; Pashley, R. M. *Colloids Surf., A* **2001**, *182*, 285−298.

(13) Abela, M.; Wattsa, J.; Digby, R. *Int. J. Adhes. Adhes.* **1998**, *18* (3), 179−192.

(14) Liakosa, I.; McAlpineb, E.; Chen, X.; Newmand, R.; Alexander, M. *Appl. Surf. Sci.* **2008**, *255* (5), 3276−3282.

(15) Folkers, J.; Gorman, C.; Laibinis, P.; Buchholz, S.; Whitesides, G.; Nuzzo, R. *Langmuir* **1995**, *11* (3), 813−824.

(16) Crouse, C.; Pierce, C.; Spowart, J. *ACS Appl. Mater. Interfaces* **2010**, *2*, 2560−2569.

(17) Weibel, D.; Michels, A.; Feil, A.; Amaral, L.; Teixeria, S.; Horowitz, F. *J. Phys. Chem. C* **2010**, *114* (31), 13219−13225.

(18) Valliappan, S.; Swiatkiewicz, J.; Puszynski, J. *Powder Technol.* **2005**, *156*, 164−169.

(19) Thiruvengadathan, R.; Bezmelnitsyn, A.; Apperson, S.; Staley, C.; Redner, P.; Balas, W.; Nicolich, S.; Kapoor, D.; Gangopadhyaya, K. *Combust. Flame* **2011**, *158*, 964−978.

(20) Dikici, B.; Dean, S.; Pantoya, M.; Levitas, V.; Jouet, J. *Energy Fuels* **2009**, *23*, 4231−4235.

(21) *CRC Handbook of Chemistry and Physics*, 71st ed.; CRC Press: Boca Raton, FL, 1991.

(22) Horn, J.; Lightstone, J.; Carney, J.; Jouet, J. *Shock Compression of Condensed Matter*, Proceedings of the Conference of the American Physical Society Topical Group, Chicago, Illinois, 2011.

(23) Bockmon, B.; Pantoya, M.; Son, S.; Asay, B.; Mang, J. *J. Appl. Phys.* **2005**, *98* (6), 064903−064907.

(24) Yarrington, C.; Son, S.; Foley, T.; Obrey, S.; Pacheo, A. *Propellants, Explos., Pyrotech.* **2011**, *36* (6), 551−557.

(25) Weismiller, M.; Malchi, J.; Lee, J.; Yetter, R.; Foley, T. *Proc. Combust. Inst.* **2011**, *33* (2), 1989−1996.

(26) Kappagantula, K.; Pantoya, M. *Energy Fuels* **2011**, *25* (2), 640−646.

(27) Starink, M. J. *Int. Mater. Rev.* **2004**, *49* (3), 191−226.

(28) Bae, J.; Kim, D.; Jeong, T.; Kim, H. *Thin Solid Films* **2010**, *518*, 6205−6209.

(29) Sun, J.; Pantoya, M.; Simon, S. *Thermochim. Acta* **2006**, *444*, 117−127.

(30) Stamatis, D.; Dreizen, E.; Higa, K. *J. Propul. Power* **2011**, *27*, 1079−1086.

(31) Osborne, D.; Pantoya, M. *Combust. Sci. Technol.* **2007**, *179* (8), 1467−1480.

(32) Solomons, T.; Fryhle, T. *Organic Chemistry*; John Wiley and Sons: Hoboken, NJ, 2011.

(33) Pantoya, M.; Dean, S. *Thermochim. Acta* **2009**, *493*, 109−110.

(34) Thadhani, N.; Namjoshi, S.; Vandersall, K.; Xu, X. *Thermal Analysis Instrumentation for the Kinetics of Shocked Materials*; Georgia Institute of Technology: Atlanta, GA, 1999.

24475

dx.doi.org/10.1021/jp308620t | *J. Phys. Chem. C* 2012, 116, 24469−24475